Prediction and measurement of leaky dielectric drop interactions

Jeremy I. Kach, Lynn M. Walker, and Aditya S. Khair*
Department of Chemical Engineering, Carnegie Mellon University, Pittsburgh, Pennsylvania 15213, USA

(Received 16 June 2021; accepted 21 December 2021; published 11 January 2022)

Application of an electric field across the curved interface of two fluids of low but nonzero conductivities, or "leaky dielectrics," can give rise to electric stresses that drive sustained fluid flow. In a uniform dc electric field of sufficiently weak magnitude, the electric and velocity fields around an isolated, neutrally buoyant leaky dielectric drop at zero Reynolds number are fore-aft and azimuthally symmetric about the applied field axis. Consequently, the drop remains stationary. The presence of a second drop breaks these symmetries, resulting in the relative motion of the drop pair. Recently, Sorgentone *et al.* derived an analytical expression for the relative velocity of a pair of widely separated drops of identical constitution, asymptotic in the inverse separation distance between the drop centroids [C. Sorgentone, J. I. Kach, A. S. Khair, L. M. Walker, and P. M. Vlahovska, Numerical and asymptotic analysis of the three-dimensional electrohydrodynamic interactions of drop pairs, J. Fluid Mech. **914**, A24 (2021)]. In the present work, we generalize the theory of Sorgentone *et al.* to interactions of dissimilar drops (of different size or constitution), and the pairwise additive interactions of three or more drops. We perform experiments on silicone oil drops suspended in castor oil, and we compare to asymptotic predictions of the drop pair trajectories. Experimental trajectories of drops with their line of centers initially at an arbitrary angle to the field direction are shown to be qualitatively predicted by our theory. We show results of experiments of dissimilar drops and of three and four drops, again observing qualitative agreement with our theoretical predictions.

DOI: 10.1103/PhysRevFluids.7.013701

I. INTRODUCTION

The application of an electric field across the interface between low-conductivity (leaky dielectric) fluids gives rise to stresses that can deform the interface and drive electrohydrodynamic (EHD) flows [1,2]. EHD flows find applications in electrosprays [3,4], electrocoalescence [5,6], electrorheology [7,8], microfluidics [9,10], the formation of Janus capsules [11], and have shown promise in improving existing methods of inkjet printing [12–14]. Much of the literature on electrohydrodynamics has focused on the deformation and breakup of drops [4,15–26]. In particular, the dynamics of drops that deform to an oblate shape has garnered recent interest [27–30]. While the dynamics of a single drop is well understood [26], many applications involve multiple drops. In electrocoalescence, for example, it is important to predict the behavior of multiple drops in electric fields weak enough to avoid breakup. To this end, the electrohydrodynamic interactions between drops must be determined.

Due to the nonzero electrical conductivities of leaky dielectrics, a drop interface polarizes in an electric field due to both free-charge accumulation and the permittivity mismatch between drop and suspending phases. The resulting surface charge profile induces an electrical stress both normal and tangential to the local interface, thus shearing the interface and driving flow in and outside of

*akhair@andrew.cmu.edu

 ©2022 American Physical Society

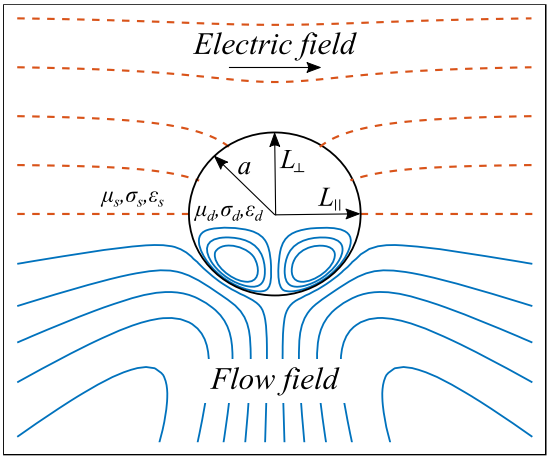

FIG. 1. Example of steady electric and velocity fields around a leaky dielectric drop in a uniform electric field, where $M = 2,\ R = 1/5,\ S = 1/3$. In this example, the drop is slightly deformed to a prolate spheroid with undeformed radius a, major axis $L_\parallel$, and minor axis $L_\perp$ with respect to the applied field direction. The viscosity μ, conductivity σ, and permittivity ε of the drop phase are denoted with subscript d, and the suspending phase properties are denoted with subscript s. Both the electric and flow fields have fore-aft symmetry about the drop equator perpendicular to the applied field direction and are axially symmetric about the poles in parallel to the applied field direction. Internal electric field lines are omitted, however the internal field is uniform and parallel to the applied field direction.

the drop. Here, by a "weak" electric field it is meant that the capillary number $\mathrm{Ca} = \mu_s U_{\mathrm{EHD}}/\gamma = \varepsilon_s E_\infty^2 a/\gamma \ll 1$, where μ_s is the viscosity of the suspending fluid, $U_{\mathrm{EHD}} = \varepsilon_s E_\infty^2 a/\mu_s$ is the velocity scale of the EHD flow, E_∞ is the strength of the applied field, ε_s is the absolute electrical permittivity of the suspending phase, a is the undeformed drop radius, and γ is the surface tension of the interface. Since U_{EHD} depends inversely on viscosity, Ca is independent of viscosity, unlike for a drop in an externally imposed flow field where the capillary number is inversely proportional to viscosity. A neutrally buoyant drop at zero Reynolds number remains nearly spherical, deforming to a spheroidal shape to leading order in Ca. Ignoring surface charge convection, the deformation of a single drop can be described to leading order in Ca using the material property ratios of viscosity $M = \mu_d/\mu_s$, conductivity $R = \sigma_s/\sigma_d$, and permittivity $S = \varepsilon_d/\varepsilon_s$, where subscripts d and s denote the drop and suspending phases, respectively. The deformation parameter, a function of the length of the major and minor axes of the drop ($L_\parallel$ and $L_\perp$, respectively), is given by the following expression derived by Taylor [15]:

$$D_T \equiv \frac{L_\parallel - L_\perp}{L_\parallel + L_\perp} = \frac{9\ \mathrm{Ca}}{16(1+2R^2)}\left[\frac{3(2+3M)}{5(1+M)}R(1-RS) + R^2(1-2S) + 1\right] + O(\mathrm{Ca}^2). \quad (1)$$

Thus, drops can either deform to a prolate ($D_T > 0$) or an oblate ($D_T < 0$) spheroid, depending solely on the properties of the fluids. An example of the steady deformation and electric and velocity fields around a single leaky dielectric drop for $M = 2,\ R = 1/5,\ S = 1/3$ is shown in Fig. 1.

Due to the fore-aft and axial symmetry of the electric and flow fields in and outside a drop, a single, freely suspended drop remains stationary. In the presence of a second drop, however, those symmetries are broken, and the drops translate by action of the flow and nonuniform electric field due to the presence of the other drop. When perfectly dielectric or conducting drops are suspended in a dielectric medium, they interact only through dielectrophoresis (DEP), i.e., the force on a body residing in an electric field gradient [31,32]. The electrostatic interaction of two dielectric spheres arbitrarily placed in an electric field was calculated using a multipole reexpansion by Washizu

and Jones [33], who found that the interaction of widely separated spheres matches closely with a point-dipole approximation [34]. In both cases, there is a critical angle between the line of centers connecting the drops and the applied field direction, $\Theta = 54.7^\circ$, below which the spheres will attract and above which they will repel. This is the basis for electrocoalescence, where these interactions are exploited to augment the rates of collision and coalescence of water drops in oil [35,36]. When the drop and suspending fluids are leaky dielectrics, the drops interact through EHD as well. This was first addressed by Sozou [37], who calculated that the flow field around two drops can be modified considerably depending on the drops' separation distance using a multipole expansion in bispherical coordinates; however, this calculation was restricted to the case of two identical, spherical drops with the line connecting their centers aligned in the direction of the applied field. Baygents, Rivette, and Stone [38] then demonstrated that leaky dielectric drops interact through a combination of EHD and DEP. They employed a boundary integral method, which considered the relative motion and deformation of identical drops aligned in the field direction. Their analysis showed that for widely separated drops, the DEP force scales to leading order as $O(a^4/d^4)$ while the EHD flow scales to leading order as $O(a^2/d^2)$, where a is the radius of the drops and d is the separation distance of their centroids. Recently, Zabarankin [39] derived an analytical expression via a multipole reexpansion for the velocities of nearly spherical but nonidentical drops aligned in the direction of the electric field. This theory matched observations by Baygents *et al.* that prolate-deforming drops may attract when drops are close and DEP dominates, yet they may repel at larger separations where the EHD flow dominates. Furthermore, Zabarankin's work introduced the possibility that oblate-deforming drops with dissimilar permittivities and conductivities in an inviscid suspending fluid could have a repulsive interaction, a behavior not reported in previous studies.

To study the EHD interactions of drops in two dimensions, Dong and Sau [40] performed lattice Boltzmann computations, using a point-dipole approximation for the DEP interaction. At a separation of $d/a = 5$ and $\mathrm{Ca} = 0.18$, they noted that the critical angle of the EHD flow for circular drops is similar to that of the point-dipole approximation for DEP. Mhatre *et al.* [41] compared boundary integral simulations to experimental drop trajectories for two drops aligned parallel to the field. Although they did not compare their simulations to experiments for drops misaligned with the field, they did experimentally observe the existence of a critical Θ, above which drops did not attract each other. More recently, Sorgentone *et al.* [42] considered three-dimensional EHD drop interactions via asymptotic theory and boundary integral simulations. Accurate to $O(a^5/d^5)$, their asymptotic theory showed that leaky dielectric drops initially at an angle to the field may align either parallel or perpendicular to the field direction depending only on the material properties of the drop and suspending phase. An expression, denoted by Φ, was derived that quantifies the competition between EHD and DEP. This expression, given again in Eq. (14), can be used to determine the long-term behavior of the drop pair. Additionally, a derived expression for a critical separation distance further quantified the competition between the DEP and EHD effects driving the interaction.

In the present work, we first extend the theory of Sorgentone *et al.* to consider nonidentical and multiple drops, widely separated. We then compare our calculations to experiments of two or more drops, showing in particular that a pairwise additive approximation is capable of qualitatively predicting the trajectories of multiple leaky dielectric drops. In Sec. II, we formulate the problem of interest. In Sec. III, the asymptotic theory for drop interactions is generalized to include dissimilar drops and multiple drops. In Sec. IV, we outline the experimental method and discuss the implications of the parameter Φ on practical systems. In Sec. V, we compare the theory to experimental measurements of drop trajectories. We first compare the theory to measurements of drop pair trajectories for identical drops, which qualitatively validate the calculations and illustrate the importance of considering the combined effects of DEP and EHD in drop interactions. We then compare the theory to experimental measurements of the trajectories of drops of different size, and we discuss the dynamics of electrically dissimilar drops. Finally, we compare the theory to

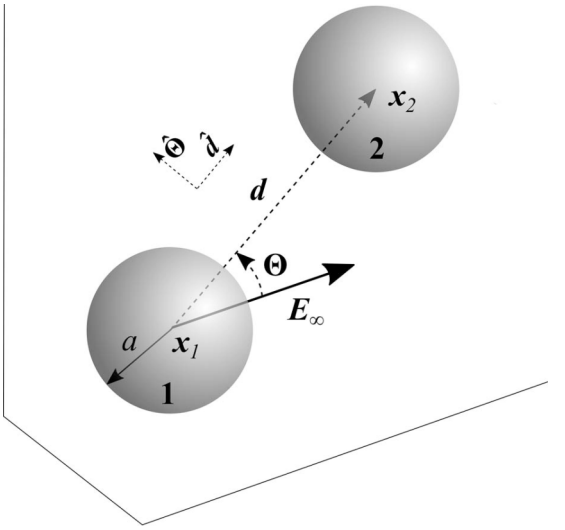

FIG. 2. Depiction of a coordinate system for two spherical drops of radius a. The centers of the drops are separated by a distance d, with the angle between the line of centers and the applied field denoted as Θ.

experimental measurements of the interactions of three and four drops. In Sec. VI, we provide the conclusions of our work.

II. PROBLEM FORMULATION

Consider two spherical, leaky dielectric drops suspended in an unbounded, density matched fluid and subject to a uniform dc electric field $\boldsymbol{E}_\infty$ pointing in direction $\hat{\boldsymbol{E}}_\infty = \boldsymbol{E}_\infty/E_\infty$. We introduce the subscripts i and j to identify the drops, where $i = 1, 2$, $j = 1, 2$, and $j \neq i$. The drop phases (denoted by subscript d) and suspending medium (denoted by subscript s) have constant and homogeneous properties of conductivity, permittivity, and viscosity, with ratios of material properties $M_i = \mu_{d,i}/\mu_s$, $R_i = \sigma_{s,i}/\sigma_d$, and $S_i = \varepsilon_{d,i}/\varepsilon_s$, respectively. The positions of the drops evolve on the timescale $\tau_c = a/U_{\mathrm{EHD}} = \mu_s/\varepsilon_s E_\infty^2$. A schematic of the two-drop system is shown in Fig. 2, where the centers of each drop, relative to an arbitrary origin, are denoted as $\boldsymbol{x}_1$ and $\boldsymbol{x}_2$.

The vector $\boldsymbol{d} = \boldsymbol{x}_2 - \boldsymbol{x}_1$ points from the center of drop 1 to the center of drop 2 with associated unit vector $\hat{\boldsymbol{d}}$. A second, right-handed unit vector $\hat{\boldsymbol{\Theta}}$ is introduced to denote rotations of $\hat{\boldsymbol{d}}$. In effect, $\hat{\boldsymbol{\Theta}}$ describes rotations of the drop pair, where a positive $\boldsymbol{\Theta}$ indicates a counterclockwise rotation of drop 2 about drop 1.

We describe the combined electrostatic and hydrodynamic problems using the approach of Melcher and Taylor [1]. We assume no free charge in the bulk, such that the potential inside and outside the drops satisfies Laplace's equation,

$$\nabla^2 \phi_i = 0, \quad \nabla^2 \phi_s = 0. \tag{2}$$

The electric field is expressed as the negative gradient of the potential, $\boldsymbol{E} = -\nabla\phi$. Far from the drops, the electric field approaches the imposed field, $\boldsymbol{E}_\infty$, and the field is bounded at the centroid of each drop. The capillary number is taken to be small, $\mathrm{Ca} \ll 1$, such that the interface of the drops can be assumed to be spherical. The potential is continuous across the surface of the drops, and the surface charge density is given as

$$\varepsilon_s(\nabla\phi_s \cdot \boldsymbol{n}_i - S\nabla\phi_i \cdot \boldsymbol{n}_i) = -q \ \text{ at } \ r_i = |\boldsymbol{x} - \boldsymbol{x}_i| = a, \tag{3}$$

where $\boldsymbol{n}_i$ is the outward pointing unit normal vector of the drops. Neglecting surface charge convection and charge relaxation, current across the interface is conserved, satisfying

$$\nabla\phi_i = R\nabla\phi_s \ \text{ at } \ r_i = a. \tag{4}$$

The assumption of no surface charge convection requires the electric Reynolds number, $\mathrm{Re}_E = \varepsilon_s^2 E_\infty^2/\sigma_s\mu_s \ll 1$. The charge relaxation timescales in and outside the drop are assumed to be small, $\varepsilon_{d,s}/\sigma_{d,s} \ll 1$.

Assuming creeping flow of incompressible fluids, the velocity and pressure inside and outside the drops are governed by the Stokes equations,

$$\nabla\cdot\boldsymbol{\sigma}_i = \mu_i\nabla^2\boldsymbol{u}_i - \nabla p_i = 0, \ \ \nabla\cdot\boldsymbol{\sigma}_s = \mu_s\nabla^2\boldsymbol{u}_s - \nabla p_s = 0, \tag{5}$$

where $\boldsymbol{\sigma} = -p\mathrm{I} + \mu(\nabla\boldsymbol{u} + (\nabla\boldsymbol{u})^T)$ is the hydrodynamic stress tensor, and I is the identity tensor. The flow is quiescent far from the drops and bounded within. The velocity is continuous across the interface, with no penetration of fluid across the boundary. The electric field acting on the developed surface charge induces a tangential Maxwell stress at the surface, which drives the EHD flow. The tangential stress balance is given as

$$[\boldsymbol{\sigma}_s\cdot\boldsymbol{n}_i - \boldsymbol{\sigma}_i\cdot\boldsymbol{n}_i]\times\boldsymbol{n}_i = q\nabla\phi_i\times\boldsymbol{n}_i, \ \ r_i = a, \tag{6}$$

where $\nabla\phi_i\times\boldsymbol{n}_i$ is the tangential component of the electric field, which is continuous across the interface. Solution of the above equations and boundary conditions gives the electric and flow fields around each drop individually, which are then used with the method of reflections to determine the interaction of widely separated drops.

III. ASYMPTOTIC APPROXIMATION OF PAIR INTERACTION

We generalize the methodology of Sorgentone *et al.* [42] to determine the interaction between two widely separated, dissimilar, leaky dielectric drops. Via the method of reflections, a single reflection of the electric and velocity fields around drop i as seen by drop j a distance d away is [43]

$$\boldsymbol{E}_i = \boldsymbol{E}_\infty - \frac{1-R_i}{1+2R_i}\,\boldsymbol{E}_\infty\cdot(\mathbf{I}-3\hat{\boldsymbol{d}}\hat{\boldsymbol{d}})\Big(\frac{a_i}{d}\Big)^3 + O\Big(\Big(\frac{a_i}{d}\Big)^6\Big), \tag{7}$$

$$\boldsymbol{u}_i = \frac{9}{10}\frac{\varepsilon_s E_\infty^2 a_i}{\mu_s}\frac{R_i(R_iS_i-1)}{(1+2R_i)^2(1+M_i)}\hat{\boldsymbol{E}}_\infty\hat{\boldsymbol{E}}_\infty : \Big[(\mathbf{I}-3\hat{\boldsymbol{d}}\hat{\boldsymbol{d}})\Big(\frac{a_i}{d}\Big)^2\hat{\boldsymbol{d}} + \frac{1}{3}\nabla\Big(\mathbf{I}\Big(\frac{a_i}{d}\Big)^3 - 3\hat{\boldsymbol{d}}\hat{\boldsymbol{d}}\Big(\frac{a_i}{d}\Big)^3\Big)\Big] + O\Big(\Big(\frac{a_i}{d}\Big)^5\Big). \tag{8}$$

The electric and flow fields have fore-aft symmetry about the equator and axial symmetry about the field direction, illustrated by the field lines and streamlines in Fig. 1, and a single drop undergoes no translational motion. Upon addition of a second drop, that symmetry is broken. The disturbance electric and velocity fields from one drop act on the other, and vice versa, resulting in translational motion of the drops.

To describe the interactions between drops, we introduce the notation $\boldsymbol{F}_{ji}$ and $\boldsymbol{U}_{ji}$, where the subscripts denotes the force or velocity on drop j due to its interaction with drop i. Approximating each drop as a point dipole, the DEP force on drop j in the disturbance electric field of drop i is

$$\boldsymbol{F}_{ji} = \boldsymbol{P}_j\cdot\nabla\boldsymbol{E}_i|_{\boldsymbol{x}=\boldsymbol{x}_j}, \tag{9}$$

where $\boldsymbol{P}_j$ is the polarizability of drop j, $\boldsymbol{P}_j = 4\pi\varepsilon_s a_j^3\frac{1-R_j}{1+2R_j}\boldsymbol{E}_\infty$, and $\nabla\boldsymbol{E}_i|_{\boldsymbol{x}=x_j}$ is the gradient of the electric field around drop i evaluated at the center of drop j. The translational velocity of drop j, considering the EHD and DEP interactions with drop i, as well as the drag on drop j, is then, via

Faxén's law for drops [44],

$$\boldsymbol{U}_{ji} = \left(1 + \frac{a_j^2 M_j}{2(2+3M_j)}\nabla^2\right)\boldsymbol{u}_i(\boldsymbol{x})|_{\boldsymbol{x}=\boldsymbol{x}_j} + \frac{1}{2\pi\mu_s a_j}\frac{1+M_j}{2+3M_j}\boldsymbol{F}_{ji}. \tag{10}$$

Insertion of Eqs. (8) and (9) into (10) returns the velocity of each drop,

$$\begin{aligned}\boldsymbol{U}_{ji} = \frac{9}{5}\frac{\varepsilon_s E_\infty^2 a_i}{\mu_s}\Bigg[&\frac{R_i(1-R_iS_i)}{(1+2R_i)^2(1+M_i)}P_2(\cos\Theta)\left(\frac{a_i}{d}\right)^2\hat{\boldsymbol{d}}\\ &- \frac{R_i(1-R_iS_i)}{(1+2R_i)^2(1+M_i)}\left(P_2(\cos\Theta)\hat{\boldsymbol{d}} + \frac{1}{2}\sin(2\Theta)\hat{\boldsymbol{\Theta}}\right)\left(\frac{a_i}{d}\right)^4\\ &- \left(\frac{3M_j}{(2+3M_j)}\frac{R_i(1-S_iR_i)}{(1+2R_i)^2(1+M_i)} + \frac{20}{3}\frac{(1+M_j)}{(2+3M_j)}\frac{(1-R_j)}{(1+2R_j)}\frac{(1-R_i)}{(1+2R_i)}\right)\\ &\times\left(P_2(\cos\Theta)\hat{\boldsymbol{d}} + \frac{1}{2}\sin(2\Theta)\hat{\boldsymbol{\Theta}}\right)\left(\frac{a_i^2a_j^2}{d^4}\right)\Bigg] + O\left(\frac{a_i^2a_j^3}{d^5}\right),\end{aligned} \tag{11}$$

where $P_2(\cos\Theta)$ is the second Legendre polynomial. Clearly, for nonidentical drops, the relative velocity of the drop pair $\boldsymbol{U}_d = \boldsymbol{U}_{ji} - \boldsymbol{U}_{ij} \neq 2\boldsymbol{U}_{ji}$, analogous to nonreciprocal interactions of phoretic particles with different interaction potentials [45,46]. For dissimilar drops, the higher-order, i.e., $O(a^4/d^4)$, interactions depend on properties from both drops i and j, as seen in Eq. (11). This is a generalization of Eq. (4.8) in Sorgentone *et al.* [42], from which the orientation of an identical drop pair can be predicted based solely on the material properties of the system. The expression presented here, namely the second and third terms in Eq. (11), shows that the interactions of dissimilar drops are more complex. When one drop is much larger than the other, Eq. (11) reduces to the EHD flow profile around the larger drop, with the smaller drop effectively acting as a tracer in the EHD flow of the larger drop. For drops of equal size but different constitution, the expression governing the $O(a^4/d^4)$ interactions of the drops becomes

$$\Phi_{ji} = \frac{1}{(2+3M_j)}\left(\frac{2(1+3M_j)R_i(1-R_iS_i)}{(1+M_i)(1+2R_i)^2} + \frac{20}{3}(1+M_j)\frac{(1-R_j)(1-R_i)}{(1+2R_j)(1+2R_i)}\right), \tag{12}$$

where Φ_{ji} denotes the $O(a^4/d^4)$ contribution to the velocity of drop j due to its interaction with drop i. Equation (12) shows that two drops may align perpendicular to the electric field direction if their conductivities are larger and smaller, respectively, than the suspending phase (i.e., $R_i < 1 < R_j$). Thus, Φ_{ji}, and therefore the total interaction of the drop pair, cannot be described using Φ_i and Φ_j for interactions of identical drops of type i and j. For drops of identical size and constitution (i.e., when $M_j = M_i$, $R_j = R_i$, $S_j = S_i$, and $a_j = a_i$), $\boldsymbol{U}_d = 2\boldsymbol{U}_{ji}$, and Eqs. (11) and (12) reduce to Eqs. (4.7) and (4.8) for identical drops given by Sorgentone *et al.* [42],

$$\begin{aligned}\boldsymbol{U}_d = \frac{18}{5}\frac{\varepsilon_s E_\infty^2 a}{\mu_s}\Bigg[&\frac{R(1-RS)}{(1+2R)^2(1+M)}P_2(\cos\Theta)\left(\frac{a}{d}\right)^2\hat{\boldsymbol{d}}\\ &- \Phi\left(P_2(\cos\Theta)\hat{\boldsymbol{d}} + \frac{1}{2}\sin(2\Theta)\hat{\boldsymbol{\Theta}}\right)\left(\frac{a}{d}\right)^4\Bigg] + O\left(\left(\frac{a}{d}\right)^5\right),\end{aligned} \tag{13}$$

and

$$\Phi = \frac{1}{(2+3M)(1+2R)^2}\left(\frac{2(1+3M)R(1-RS)}{(1+M)} + \frac{20}{3}(1+M)(1-R)^2\right). \tag{14}$$

Equations (11) and (13) can be reduced to pure dielectrophoresis of conducting drops by setting $S = 1/R$, where the EHD interaction of $O(a^2/d^2)$ is absent and the weaker DEP governs the interaction of the drops to leading order of $O(a^4/d^4)$. In this case, the charging timescales of the drop and suspending phases match ($\varepsilon_d/\sigma_d = \varepsilon_s/\sigma_s$, or $RS = 1$), and the tangential electric stress

on each side of the interface balances, eliminating the driving force for the interface to shear and resulting in the EHD flow vanishing, exemplified by $\boldsymbol{u}_i = \boldsymbol{0}$ when $RS = 1$ in Eq. (8).

The relative velocity of the drop pair can be used to determine the trajectory of the drop pair via the relations

$$\frac{\mathrm{d}d}{\mathrm{d}t} = \boldsymbol{U}_d \cdot \hat{\boldsymbol{d}} \quad \text{and} \quad d\frac{\mathrm{d}\Theta}{\mathrm{d}t} = \boldsymbol{U}_d \cdot \hat{\boldsymbol{\Theta}}, \tag{15}$$

where d is the separation distance between the centroids of the drops, and Θ is the angle between the drops' line of centers and the electric field direction, equal to $\arccos(\hat{\boldsymbol{E}}_\infty \cdot \hat{\boldsymbol{d}})$. The unit vectors $\hat{\boldsymbol{d}}$ and $\hat{\boldsymbol{\Theta}}$ are those pointing along the line of centers of the drops and perpendicular to the drops' line of centers. Additionally, the position of each drop can be tracked individually as

$$\frac{\mathrm{d}\boldsymbol{x}_j}{\mathrm{d}t} = \boldsymbol{U}_{ji}, \tag{16}$$

which, while a trivial result, can be extended to predict the behavior of multiple drops, as follows. When there are multiple drops, it is assumed that each drop moves due to pairwise interactions with every other drop. The position of each drop can then be predicted by summing over the interactions of that drop with all other drops. This yields the same expression as Eq. (16), but now including a sum over i. The positions of the entire collection of drops can then be described as

$$\frac{\mathrm{d}\boldsymbol{x}_j}{\mathrm{d}t} = \sum_{i \neq j}^{N} \boldsymbol{U}_{ji} \text{ for } j = 1, 2, \ldots, N, \tag{17}$$

where $\boldsymbol{x}_j$ is the position of the jth drop, $\boldsymbol{U}_{ji}$ is the velocity of drop j due to its interaction with drop i, and N is the total number of drops in the system.

The trajectories of a set of two or more drops can be predicted via integration of Eq. (17). The positions of the drops in time are hence calculated by numerically integrating Eq. (17) using a forward Euler scheme with time step $0.001t_c$, where $t_c = \mu_s/\varepsilon_s E_\infty^2$ is the characteristic timescale of the EHD flow. In the next sections, these calculated trajectories are compared to experimental results in various scenarios, and theoretical results for other scenarios are shown as well.

IV. MATERIALS AND METHODS

Experiments were performed in a 3D-printed acrylic cell of 2.8 cm width ×3.6 cm length ×7 cm height developed by Sengupta *et al.* [47]. Two stainless-steel electrodes 35 mm wide are set 28 mm apart. Voltages of 2, 3, 4, and 5 kV are applied to one electrode from a high-voltage power supply (Gamma High Voltage Research, Inc.) with the other grounded, resulting in calculated electric field strengths of 0.714, 1.07, 1.43, and 1.79 kV/cm, respectively, in the cell. A foot switch connected to the voltage supply circuit allows for rapid and safe activation/deactivation of the electric field. Drops of volume 1 μL (620 μm radius) are administered using a 25 μL glass syringe with a grounded 22 s gauge stainless-steel needle (Hamilton). After insertion into the cell, drops are then placed in their initial positions by moving nearby fluid using the grounded needle. The two walls adjacent to the electrodes have circular windows, where drops are imaged using a camera (Point Grey Grasshopper) with a 10× objective lens (Nikon) and a fiber optic back light (QVABL, Dolan-Jenner). The drops are initially placed in the same focal plane. Via Eq. (11), drops positioned in the plane made by the field direction and the line connecting their centers will only move within that plane. Visual observations made during the experiments indicate that out-of-plane motion is small compared to that in-plane. A schematic of the setup is shown in Fig. 3. Images are recorded at 7 frames per second with LabView. Drop positions and trajectories are analyzed in MATLAB with the function *imfindcircles*; the data are smoothed for clarity by taking a moving average of the previous seven data points, and data points spaced 1 s apart are shown.

The oils used are 350 cSt silicone oil (Sigma-Aldrich) and castor oil (Sigma-Aldrich). Prediction of the interaction between drops requires accurate knowledge of the drop and suspending phase

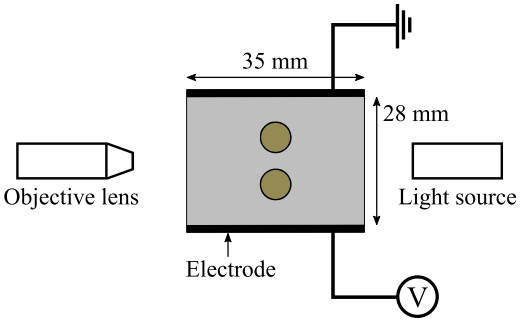

FIG. 3. Schematic of the experimental setup. Drops are initially placed in the same focal plane, where they tend to remain throughout the experiment.

fluid and electrical properties. Electrical properties are taken from Lanauze *et al.* [23], wherein electrical impedance spectroscopy was used [48], and the viscosities of the fluids are measured using a concentric cylinder rheometer (DH-2, TA Instruments) at 20 °C. The densities are considered as given by the supplier. These material properties are given in Table I.

For identical drops, the quantity $1 - RS$ and the expression for Φ in Eq. (14) are enough to qualitatively predict how a given pair of drops will behave. The leading-order term in Eq. (13) determines the relative velocity of the drop pair at large separation distances. This term is purely electrohydrodynamic, since it vanishes if $1 - RS = 0$. The sign of $1 - RS$ determines the direction of this EHD interaction, where if $1 - RS > 0$ (<0), $\boldsymbol{U}_d > 0$ (<0), and widely separated drops will repel (attract) when $P_2(\cos\Theta) > 0$, or $\Theta < 54.7°$, and attract (repel) when $\Theta > 54.7°$. The shorter-range $O(a^4/d^4)$ contribution to the relative velocity is due to a combination of both EHD and DEP. The expression Φ quantifies the interplay between EHD and DEP interactions, and can be used with the sign of $1 - RS$ to predict whether a drop pair will come together or drift apart. From Eq. (13), the only contribution to the drop pair orientation relative to the field is scaled by $-\Phi$. As indicated in Fig. 2, positive motion in the $\hat{\boldsymbol{\Theta}}$ direction constitutes a rotation toward a perpendicular alignment relative to the field. Thus, just by knowing the sign of Φ, the direction the drop pair aligns can be predicted. Finally, to qualitatively approximate the dependence of the pair interaction on separation distance, Sorgentone *et al.* introduced a critical separation distance, d_c, solved by setting $\boldsymbol{U}_d = 0$ and $\Theta = 0$ or $\pi/2$. From Sorgentone *et al.* [42],

$$\frac{d_c}{a} = \sqrt{\frac{(1+2R)^2(1+M)}{R(1-RS)}\Phi}. \tag{18}$$

The critical separation distance d_c gives the centroid separation where the effects of EHD and DEP balance, and it is an equilibrium point where the drops do not move relative to each other. Above this separation distance, long-range EHD interactions will dominate, and below this separation distance the drop motion will be dominated by DEP. The combined use of $1 - RS$, Φ, and d_c to predict the long-time behavior of a leaky dielectric drop pair can be visualized as a phase diagram for a chosen value of one of the three material property ratios. For $M = 1$, the associated phase diagram

TABLE I. Material properties for a silicone oil drop suspended in castor oil. Here, ε denotes the relative permittivity.

Fluid	ε	σ (S/m)	μ (Pa s)	ρ (kg/m^3)
Castor oil	4.9	5.8×10^{-11}	0.99	961
Silicone oil	2.8	2.0×10^{-12}	0.39	970

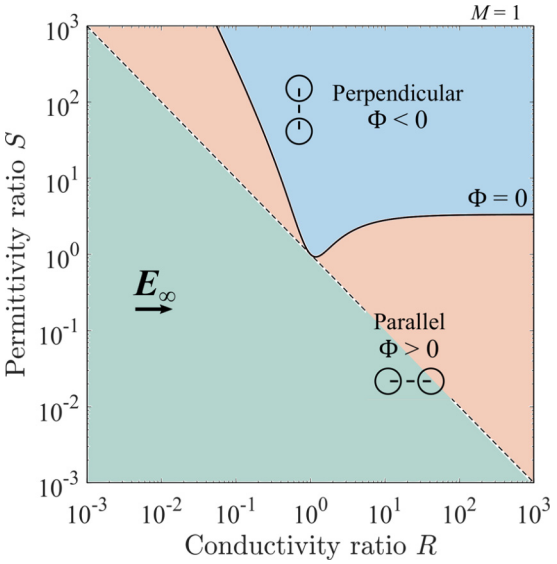

FIG. 4. Phase diagram for the behavior of a pair of equiviscous ($M = 1$), identical, leaky dielectric drops with permittivity ratio S and conductivity ratio R, based on Eq. (4.8) from Sorgentone *et al.* [42]. The solid black line denotes combinations of S and R for which $\Phi = 0$ and the orientation of the drops is steady in time. In the (blue) region above the black line, $\Phi < 0$, such that material systems in that region will show drop pair rotation toward $\Theta = \pi/2$. Below the black line, $\Phi > 0$. In the (orange) region between the lines of $\Phi = 0$ and $RS = 1$, drop pairs will rotate toward parallel and attract when $\Theta < 54.7^\circ$. In the green region below $RS = 1$, drop pairs will rotate toward parallel, however whether they attract or repel at $\Theta < 54.7^\circ$ depends on the separation distance relative to d_c for the given M, S, and R.

is shown in Fig. 4. For systems where $\Phi < 0$, drop pairs rotate toward a perpendicular alignment with the field. The line $\Phi = 0$ never crosses $RS = 1$, thus systems where $\Phi < 0$ will always have $RS > 1$ and will repel when aligned perpendicular to the field. In these cases, d_c/a is never greater than 2, and drops will repel, however the error in prediction grows as drop separation decreases. In the region where $\Phi > 0$ and $RS > 1$, drops align parallel to the field and attract along their alignment. Here, since $1 - RS < 0$ while Φ is positive, d_c is imaginary, and the interaction behavior is directionally identical to pure DEP. When $RS < 1$, Φ is always positive, and drops align along the field direction. In this region, whether the drops repel or attract in the field direction depends on their separation distance relative to d_c. At separations above d_c drops will repel in the field direction, while below d_c they will attract, making d_c in this case an unstable equilibrium position. Therefore, the quantity $1 - RS$, Eq. (14), and Eq. (18) can be used to determine how a pair of identical drops will qualitatively behave under an electric field. For the system given in Table I, $M = 0.39$, $R = 29$, and $S = 0.57$. Although the phase diagram in Fig. 4 is for $M = 1$, not much change is observed when $M = 0.39$, placing the system of silicone oil drops suspending in castor oil in the orange region of Fig. 4. Here, the product $RS = 17 > 1$ and $\Phi = 0.53 > 0$. Thus, these drops are predicted to align parallel to the field and attract one another.

In practicality, the material properties of systems where $\Phi < 0$ are heavily constrained. As M increases from unity for Fig. 4, the line for $\Phi = 0$ on the right sight of the diagram increases in slope, making the region of S and R for which $\Phi < 0$ narrow quickly. In the EHD literature, the maximum value of S is around 40, corresponding to water ($\varepsilon \approx 80$) in oil ($\varepsilon \gtrsim 2$) [16,49–51], thus narrowing the accessible zone of the phase diagram in real systems. The dip at $S = R = 1$ remains unchanged with M. Thus, fluid combinations with similar conductivities are seemingly feasible systems to have $\Phi < 0$. These systems, however, clearly must be immiscible, with distinct permittivities, as

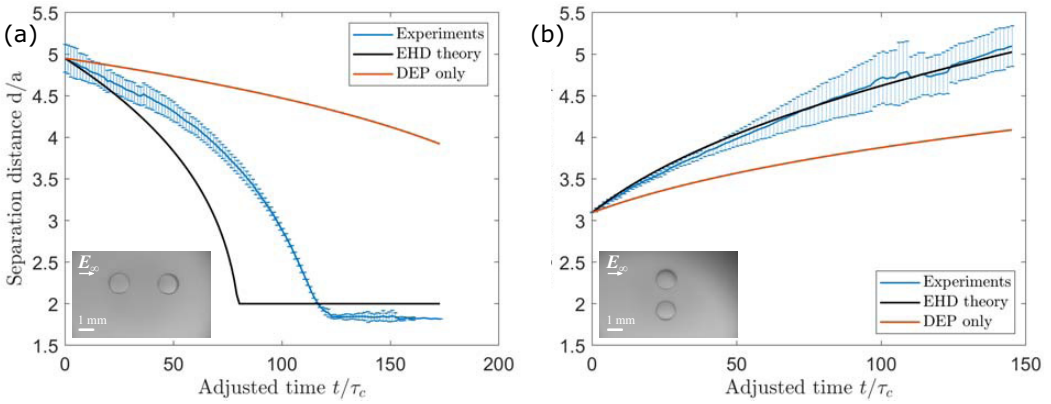

FIG. 5. (a) Centroid separation between two 350 cSt silicone oil drops in castor oil aligned parallel to the field. (b) Centroid separation between two drops aligned perpendicular to the field. Error bars represent a standard deviation of interpolated and time-averaged experiments. In both cases, $\sin(2\Theta) = 0$ and minimal rotation of the drop pair is observed. $E_\infty = 1.79$ kV/cm and $a = 620$ μm.

well as low capillary numbers and matched densities, such that the drops will not break up at field strengths needed to observe their interaction, or settle on a timescale faster than their interaction. These conditions are not wholly exclusive, however experimental evidence of interactions for drops with $\Phi < 0$ has not been reported as of this writing.

The theory presented in Sec. III relies on the assumptions that the capillary number, Reynolds number, and electric Reynolds number are small. A typical capillary number in our experiments is calculated to be $\mathrm{Ca} = 0.19$, using an initial drop radius of 620 μm and a surface tension value for castor oil and silicone oil of 4.5 mN/m from Salipante and Vlahovska [22]. Using outer phase properties of castor oil, the Reynolds number $\mathrm{Re} = 5.24 \times 10^{-4}$, and the electric Reynolds number $\mathrm{Re}_E = 1.05$. An electric Reynolds number of 1.05 indicates the effect of surface charge convection may not be negligible, however for the sake of qualitatively predicting drop interactions, we will show that use of this assumption is reasonable, and in fact variation of Re_E will be shown to have little impact on the interaction dynamics in Sec. V A.

V. RESULTS AND DISCUSSION

A. Interaction of identical drops

Results are presented of two identical silicone oil drops suspended in castor oil subject to a uniform electric field. Via Table I, the material property ratios for this system are $M = 0.39$, $R = 29$, and $S = 0.57$, thus Eq. (1) dictates that these drops will deform into oblate spheroids, where the major axis is perpendicular to the field direction. Here, the product $RS > 1$, therefore drops aligned at angles $\Theta < 54.7^\circ$ to the field should attract and drops at angles $\Theta > 54.7^\circ$ to the field should repel. In the first set of experiments, drops are initially aligned parallel ($\Theta = 0^\circ$) or perpendicular ($\Theta = 90^\circ$) to the field direction. The relative velocity and trajectory of the drop pair should then only be a function of the centroid separation d of the drops. Figures 5(a) and 5(b) show the separation distance of parallel and perpendicular aligned drops as a function of dimensionless time, respectively, where time is nondimensionalized with $\tau_c = \mu_s/\varepsilon_s E_\infty^2$. Insets in the bottom corners are pictures of the initial positions of the drops in one of the experiments included in each of the presented datasets. In these experiments, precise repeated placement of the drops in the same initial position is difficult. To analyze the data from experiments started at the same initial angle but varying separation distances, we consider the fact that the interactions between the drops are strongest (and therefore the most reproducible) the closer the drops are together. Since $\mathrm{Re} \ll 1$,

the flow is reversible, therefore the time axis of each experiment is shifted (without changing the time increment between the data points) such that the slope of separation distance versus time for each experiment reaches a minimum value at the same time, allowing a clear comparison of the trajectories between experiments. These experimental trajectories are shown with the EHD theory of Eq. (13) and the case of pure DEP ($S = 1/R$). The theoretical trajectories include a cutoff at $d/a = 2$, where a hard-sphere interaction is imposed. Clearly, considering only DEP results in a drastic underprediction of the rate of approach of the drop pair, which strongly suggests that EHD interactions are present. When drops are attracting [Fig. 5(a)], a faster approach is predicted compared to the experiments when starting at a separation distance $d/a \approx 5$. Additionally, the drops attain a minimum centroid separation of 1.8, which can be attributed to the oblate deformation of the drops, whereas perfect spheres will reach a minimum separation of 2. Prediction of the repulsive interaction between the drops, on the other hand, matches quite well with the measured trajectories. The asymptotic theory here is accurate through $O(a^4/d^4)$, and is therefore restricted to descriptions of widely separated drops, so predicted and measured trajectories should become increasingly disparate as drops come closer together. A comparison can be made to Figs. 7 and 8 in Sorgentone *et al.*, which show the asymptotic theory for identical drops along with boundary integral computations. At separations as low $d/a = 3.5$, the theory and computations are nearly identical, yet they diverge as separation distance decreases. The same divergence between the asymptotic method of reflections and a more rigorous approach like the twin multipole reexpansion can be seen in similar systems of conducting spheres in electrolyte [52]. While the asymptotic theory loses accuracy with decreasing separation distance, the error in the measured trajectories is observed to increase when drops are farther apart. This is attributed to the fact that when the drops are relatively close together, their interaction velocity is strong compared to any interfering effects, such as gravity, migrations due to field distorting impurities and charge carriers, or triboelectric charge. When the drops are farther apart, the relative strength of interaction is abated compared to the uncontrolled effects just stated, hence the widening of error bars at larger d/a in Fig. 5. Evidently, then, there is a desirable experimental range for attractive interactions around $d/a = 4$–4.5, where the pair interactions dominate in the system and the drops are separated enough for the theory to be qualitatively relevant. In light of this fact, the asymptotic theory qualitatively predicts the observed experimental trajectories quite well.

Admittedly, the electric Reynolds number of the suspending phase, $\mathrm{Re}_{E_s} = 1.05$, is not small. The drop phase value, $\mathrm{Re}_{E_d} = 25.52$, is even larger, clearly in violation of the assumption that $\mathrm{Re}_E \ll 1$. To determine the impact of Re_E and surface charge convection on the drop trajectories, experiments of parallel- and perpendicular-aligned drops were performed at various electric field strengths. The effect of surface charge convection on the interaction velocities of the drops can be visualized by normalizing the time over which the drops interact by τ_c, where E_∞, and thus τ_c, now varies between experiments. Results for drops with $\Theta = 0^\circ$ are plotted in Figs. 6(a) and 6(b), and with $\Theta = 90^\circ$ in Figs. 6(c) and 6(d). Normalization of time by τ_c collapses the trajectories together, indicating that the role of surface charge convection either has a small influence on the interactions at the separation distances shown, or the effect similarly scales with E_∞^2. It should be noted as well that Ca similarly scales with E_∞^2, however the maximum Ca achieved is 0.19, and as seen in the insets of Fig. 5 the drops remain nearly spherical. Therefore, the collapse of the trajectories in Fig. 6 justifies the choice of a 5 kV applied voltage, where the strongest possible interactions between drops can be induced without observing a change in the dynamics of their interaction. Included in Figs. 6(b) and 6(d) are dimensionless theoretical trajectories for attracting and repelling drops, respectively. There is a slight overprediction of the perpendicular drop separations, however this is consistent with Fig. 5(b). In both cases, the asymptotic theory performs reasonably well in predicting the normalized behavior of the drops, demonstrating that the physics inherent in these pairwise interactions are captured, and that using the largest voltage difference of 5 kV to conduct the experiments does not appreciably impact the dynamics of the drops.

We now consider drops unaligned with the electric field direction. Drops with an angle $\Theta \neq 0^\circ$ and $\Theta \neq 90^\circ$ will rotate due to the $O(a^4/d^4)$ EHD and DEP interactions of the drops, described by

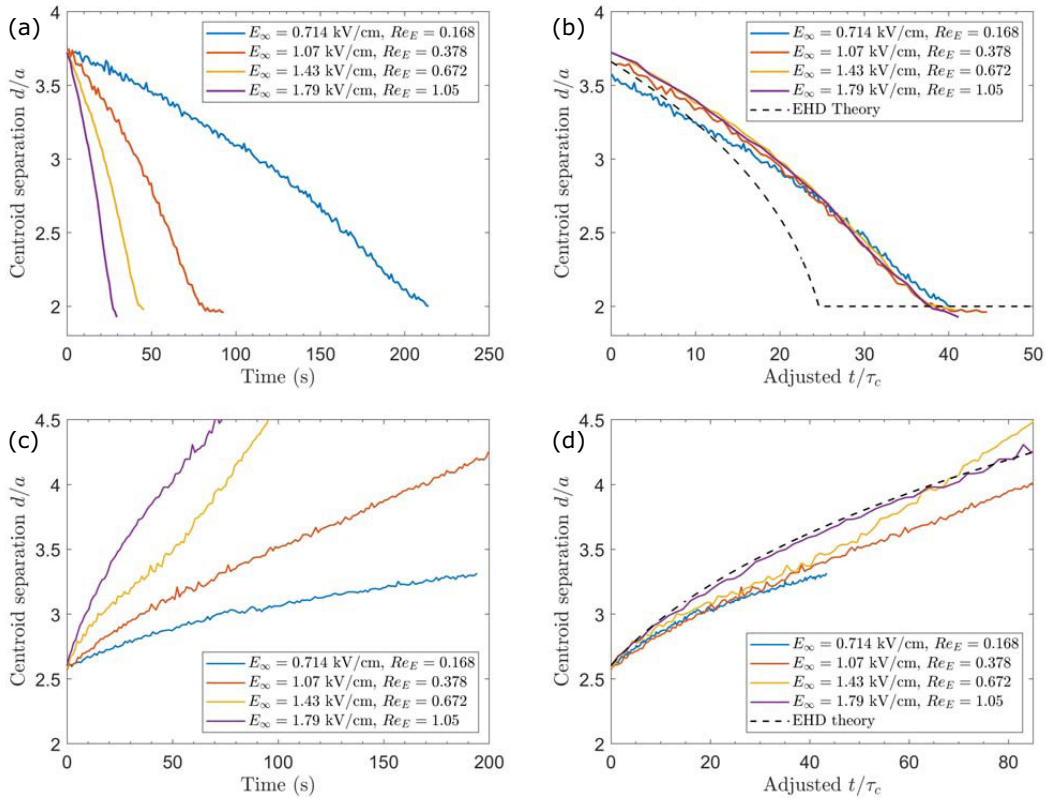

FIG. 6. Parallel and perpendicular drop trajectories for various applied voltages, with $\mathrm{Re}_E = \varepsilon_s^2 E_\infty^2/\sigma_s\mu_s$. (a) Drops are aligned parallel to the field direction. (b) The same trajectories as (a), with time normalized by τ_c. (c) Drops are aligned perpendicular to the field. (d) The same trajectories as (c), with time normalized by τ_c. Trajectories collapse upon normalization of time by $\tau_c = \mu_s/\varepsilon_s E_\infty^2$, indicating that the maximum voltage tested of 5 kV will not appreciably alter the dynamics of the drop interactions compared to lower voltages.

the $\hat{\boldsymbol{\Theta}}$ term in Eq. (13). The direction of the pair rotation can be predicted based on the discussion of Φ in Sec. IV, and here the dynamics of drop pair rotations are shown experimentally. In performing these experiments, similarly as discussed with Fig. 5, the drop interactions were stronger the closer the drops started together, while more variability was observed at larger separation distances. Like the experiments shown thus far, precisely matching initial conditions for the sake of comparison between trials is difficult. Additionally, unlike with drops aligned parallel or perpendicular to the field direction, normalizing the data between experiments starting at different initial positions proves infeasible, since the velocities of drop pairs at similar separation distances but different angles to the field (and vice versa) are not the same. In other words, drop pairs starting farther apart may not "pass through" the same position as drops starting at a similar angle to the field but closer together, rendering comparison of their trajectories impossible. Consider two experiments where drops start at the same d_0 but differ in Θ_0 between runs. The two velocities scale with the same a/d_0, but values of the second Legendre polynomial, which also scale the interaction velocity, are different. Thus, the angle that the drops' line of centers makes with the field can have a noticeable effect on the drop pair dynamics, exemplified in Fig. 7. Figures 7(a) and 7(b) are the center-to-center and angular trajectories for a drop pair with $d_0 = 4.7$ and $\Theta_0 = 21^\circ$, and Figs. 7(c) and 7(d) correspond to a drop pair with $d_0 = 4.4$ and $\Theta = 39^\circ$. Even though the drop pair in Fig. 7(a) starts at a larger initial separation distance than in Fig. 7(c), the drops closer

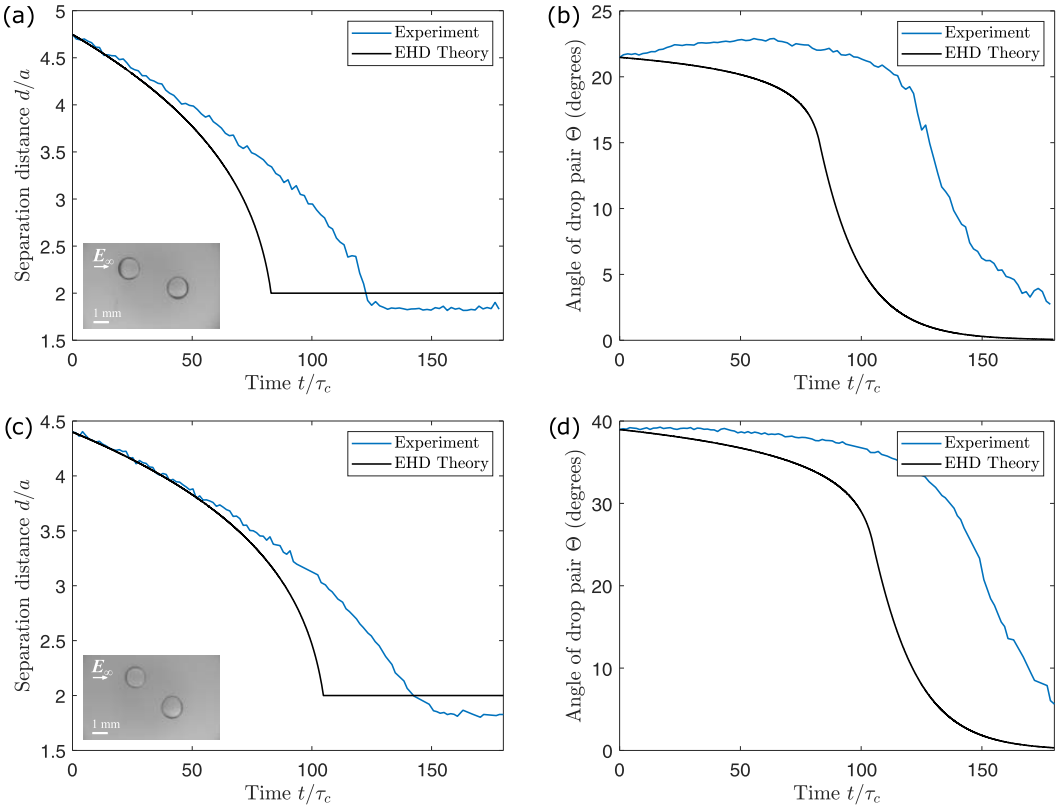

FIG. 7. (a) Separation distance between the centers of drops unaligned with the field direction, and (b) angle between the line of centers of the drops and the field direction, for drops initially placed with $d_0/a = 4.7$ and $\Theta_0 = 21^\circ$. (c) Separation distance and (d) angle between line of centers and field, for drops initially placed with $d_0/a = 4.4$ and $\Theta_0 = 39^\circ$. The vector between the drops points from the drop on the left to the one on the right, and angles plotted are $|\Theta|$ (therefore always between 0° and 90°).

together but starting at a larger Θ attract each other more slowly. The increased angle between the drop pair and the electric field results in a reduced initial relative velocity, as $P_2(\cos(21^\circ)) = 0.80$, while $P_2(\cos(39^\circ)) = 0.41$. Note that Eq. (13) is successful at predicting both the center-to-center and angular initial trajectories of the drop pairs in Fig. 7; although seemingly large, the early discrepancy in Θ between the experimental and theoretical trajectories in Fig. 7(b) is only about 3°. The prediction of Θ is seen to quickly diverge from the measured values at the same time that the predicted and measured separation distances split. The failure of Eq. (13) to quantitatively capture the dynamics of the drops at close distances is indicative of the method of reflections employed, and should not obfuscate the qualitative success of the theory in predicting drop pair behaviors. That the nature of interactions between arbitrarily positioned drops, and the timescale of their interaction, can be predicted underscores the power of the asymptotic method of reflections. Experiments are also performed of drops initially unaligned with the field at angles larger than $\Theta = 54.7^\circ$. At these angles, drop pairs will initially repel while still rotating toward the electric field direction and decreasing Θ. Upon crossing $\Theta = 54.7^\circ$, the center-to-center interaction switches from repulsive to attractive, and the drops begin to approach each other. An example of this behavior is shown in Fig. 8. The initial separation d_0/a of the drops is just over 2, and the drops rotate toward parallel and repel to a maximum of 2.9 where they reach an angle of $\Theta \approx 54.7^\circ$. At this moment, the centerline velocity of the drops is no longer repulsive, and the drops approach each other until they are near

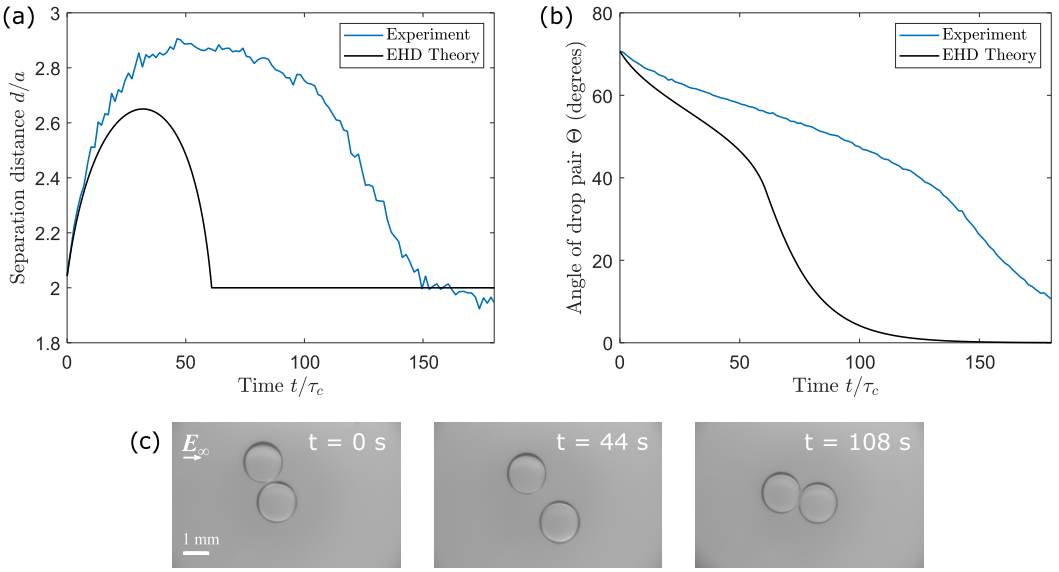

FIG. 8. (a) Separation distance between the centers of drops unaligned with the field direction, and (b) angle between the drops' line of centers and the field direction. (c) Photos taken from the experiment showing the progression of drop positions in time. At the initial time, $\Theta_0 > 54.7^\circ$, and drops initially repel. The vector between the drops points from the drop on the left to the one on the right, and angles plotted are $|\Theta|$.

contact. While these dynamics are captured with Eq. (13), the extent of repulsion and the timescale of the interaction are not in quantitative agreement. This is entirely expected to be the case with an asymptotic theory being only accurate through $O(a^4/d^4)$. Over the course of the whole experiment, the drops never reach a separation distance large enough where the error from neglected terms can be accurately ignored, and thus comparison of the data shown in Fig. 8 to the EHD theory should only be for qualitative consideration. Nonetheless, the ability to capture qualitatively the dynamics of drop pairs unaligned with the electric field, even at small separation distances, with an asymptotic theory for widely separated drops is remarkable.

B. Interaction of dissimilar drops

Here we consider the interaction of drops of different sizes and composition. When drops are differing in size, the strength of interaction of the smaller drop acting on the larger one is no longer the same as the larger drop acting on the smaller one. This is evident in the velocity scale for drop j in the presence of drop i, $U = \varepsilon E_\infty a_i/\mu_s$, scaling with the radius a_i. Due to these nonreciprocal interactions, the center of mass between the drops is not constant in time, and the relative velocity of the drop pair must be modeled with the more general expression $\boldsymbol{U}_d = |\boldsymbol{U}_{ji} - \boldsymbol{U}_{ij}|$, where $\boldsymbol{U}_{ji}$ and $\boldsymbol{U}_{ij}$ are found via Eq. (11). We compare calculation of the trajectories using Eq. (11) for two drops, one of radius $a_j = 620$ μm (same size as the previous experiments) and the other $a_i = 391$ μm (a quarter the volume of drop j, or 0.25 μL), to that for identical drops using an average radius in Eq. (13) in Fig. 9. As shown similarly for identical drops, Eq. (11) predicts the interaction of the drops reasonably well at separation distances of around $d/a_{\text{avg}} = 4$ and larger. For comparison, the trajectory is shown for identical drops using the mean size $a_{\text{avg}} = 505.5$ μm of the two dissimilar drops. Both Eq. (11) for dissimilar drops and Eq. (13) for identical, average-sized drops agree qualitatively with the experimental trajectory of the drops. Only a slight difference is observed between the two predictions, which is expected upon briefly comparing the differences in leading-order $O(a^2/d^2)$ terms of the interaction velocities. With the

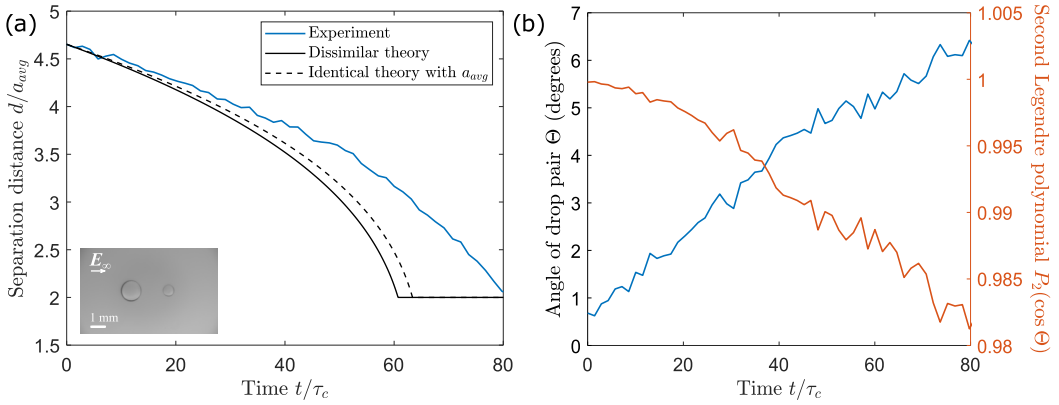

FIG. 9. (a) Normalized separation distance d/a_{avg} for drops of dissimilar size. The solid black line indicates theoretical prediction of the separation distance from Eq. (11); the dotted black line indicates the prediction for identical drops with Eq. (13) using an average radius of 505.5 μm. The inset shows the initial position of drops when electric field is applied. (b) The angle between line of centers and the field direction shown with corresponding values of the second Legendre polynomial. The largest angle observed between the line of centers and the applied field is $\Theta \approx 0.11$, which gives a value of 0.98 for the second Legendre polynomial.

drop sizes given above, the leading-order terms can be used to estimate how different predictions from Eq. (13) for identical, average-sized drops will be compared to predictions for dissimilar drops using Eq. (11). The leading-order relative velocity of identical, average-sized drops scales as $2a_{\text{avg}}^3/d_0^2$, while the leading-order relative velocity of a dissimilar drop pair scales as $a_i^3/d_0^2 + a_j^3/d_0^2$, giving the ratio of the two relative velocities, respectively, as $2a_{\text{avg}}^2/(a_i^3 + a_j^3)$. From this expression, the predicted leading-order velocity for identical, average-sized drops will always be slower than that predicted for dissimilar drops, which coincides with the faster predicted approach of dissimilar drops observed in Fig. 9. To highlight the nonreciprocal EHD interactions of the drop pair, a parallel initial configuration of the drops is chosen in order to minimize the effect of gravitational settling on the pair dynamics. We find that although there is some slight vertical misalignment of the drops, due to the larger drop settling faster than the smaller one, the drop pair only briefly reaches a maximum rotation of $\Theta \approx 6^\circ$, shown in Fig. 9. Calculation of the reduction in the interaction velocity because of this brief off-parallel alignment shows only a 2% difference in the calculated value [$P_2(\cos(6.3^\circ)) = 0.98$ versus $P_2(\cos(0)) = 1$], hence the effect of gravitational settling can be reasonably neglected. While a more precise calculation should include gravitational effects on the drop pair, Fig. 9 shows that the asymptotic theory is able to capture the EHD component of the interactions involved even when drops are of different sizes.

Unlike for differences in size shown above, small variations in material properties between the drops can lead to starkly different pair interactions. As first noted by Zabarankin [39] for drops whose line of centers is parallel to the applied field, and here for drops in arbitrary orientations via Eq. (11), two oblately deforming drops may repel along the axis of the electric field if their conductivity ratios are larger and smaller than unity (i.e., $R_i > 1 > R_j$). This counterintuitive result is indicative of the fact that the interactions between materially dissimilar drops cannot simply be predicted by knowing the interactions for identical drops of each type. This repulsive interaction results from the direction of the polarizability of the drops, determined by the Clausius-Mossotti factor $(1 - R)/(1 + 2R)$ [34]. For identical drops, the Clausius-Mossotti factors are the same, and thus the DEP force on each drop along the field axis is attractive. However, drops having Clausius-Mossotti factors of opposite sign will instead experience a repulsive DEP force along the field axis. For drops with high viscosity ratios (effectively rigid particles), or when the ratio $RS \sim 1$, the DEP interaction dominates and the drop pair will have a steady-state configuration such that the drops are in contact and aligned perpendicular to the field direction.

The interactions between drops become more complex when EHD is accounted for. Unlike with DEP, the EHD interactions of the drops are nonreciprocal, such that the center of mass of the drop pair moves in time. Additionally, as with Eq. (18) for identical drops, a critical separation distance for dissimilar drops, where DEP and EHD balance, exists as well. This critical separation distance can be written as

$$d_c = \sqrt{\frac{(\alpha_{ji} + \alpha_{ij})a_i^2 a_j^2 + \beta_i a_i^4 + \beta_j a_j^4}{\beta_i a_i^2 + \beta_j a_j^2}}, \tag{19}$$

where

$$\alpha_{ji} = \frac{3M_j}{(2+3M_j)} \frac{R_i(1-S_iR_i)}{(1+2R_i)^2(1+M_i)} + \frac{20}{3} \frac{(1+M_j)}{(2+3M_j)} \frac{(1-R_j)}{(1+2R_j)} \frac{(1-R_i)}{(1+2R_i)}$$

and

$$\beta_i = \frac{R_i(1-R_iS_i)}{(1+2R_i)^2(1+M_i)}. \tag{20}$$

Here, α_{ji} denotes the prefactor for the $a_i^2 a_j^2$ term in the velocity of drop j due to the presence of drop i given in Eq. (11), and β_i denotes the prefactor for the a_i^2 and a_i^4 terms in the velocity of drop j due to the presence of drop i. As with Eq. (18), for real values of Eq. (19), the behavior of the drop pair will be drastically different depending on if $d_0 < d_c$ or $d_0 > d_c$. The importance of considering EHD in the interactions of electrically dissimilar drops is showcased via computed trajectories in Fig. 10. Figure 10 shows three cases exemplifying the behavior described above. Here, S_i (blue) $=$ S_j (red) $= 1$, $R_i = 10$, and $R_j = 1$. The viscosity ratio and the initial position of the drops are varied between cases. Figure 10(a) shows the spacial trajectories of the dissimilar drops just described, where both drops have a viscosity ratio of $M = 10^6$. Thus, DEP interactions dominate the behavior of the drop pair, and a symmetrical interaction where the drops eventually align perpendicular to the field direction and make contact at their equators is observed. In Fig. 10(b), initial conditions of the pair remain the same, however the drops are now equiviscous with the suspending phase, and EHD plays a considerably larger role. While the ending configuration of the drop pair is the same as for the nearly rigid-particle case of Fig. 10(a), the center of mass of the pair moves in time. The paths taken by the drops illustrate the nonreciprocity of their interaction. Importantly, the time required for the drop pair to reach its minimum separation distance is more than halved when EHD is present, as shown in Fig. 10(d). Here, the DEP interaction of the drops drives the pair toward a perpendicular alignment with an initial repulsion, while the effect of the EHD interaction suppresses that initial repulsion, allowing the dynamics of the drop pair to occur at a closer separation distance where they will be stronger. The competition between EHD and DEP is made clear in Fig. 10(c), where the initial separation of the drops $d_0/a = 5.4$ is larger than the critical separation $d_c/a = 5.1$. Thus, the long-range EHD interaction dominates, and the drops are driven toward a perpendicular alignment where they repel instead of attract. Hence, as shown in Fig. 10(d), the drop pair will continue to repel after rotating above Θ_c without making contact. Figure 10 exemplifies the complexity in dissimilar drop interactions under an applied field. The interplay between EHD and DEP effects results in dynamics of the drop pair that cannot simply be predicted based on the identical interactions of each drop phase.

C. Interaction of multiple drops

Pairwise interaction calculations are commonly used to approximate the behavior of large-scale systems of drops or particles in various contexts [36,46,53–55]. To validate the use of a pairwise theory for systems of more than two drops, we compare the model to experiments of three and four identical drops. In Figs. 11 and 12, the center-to-center and angular components of Eq. (17) are shown alongside the trajectories of multiple drops. Qualitative agreement is observed between

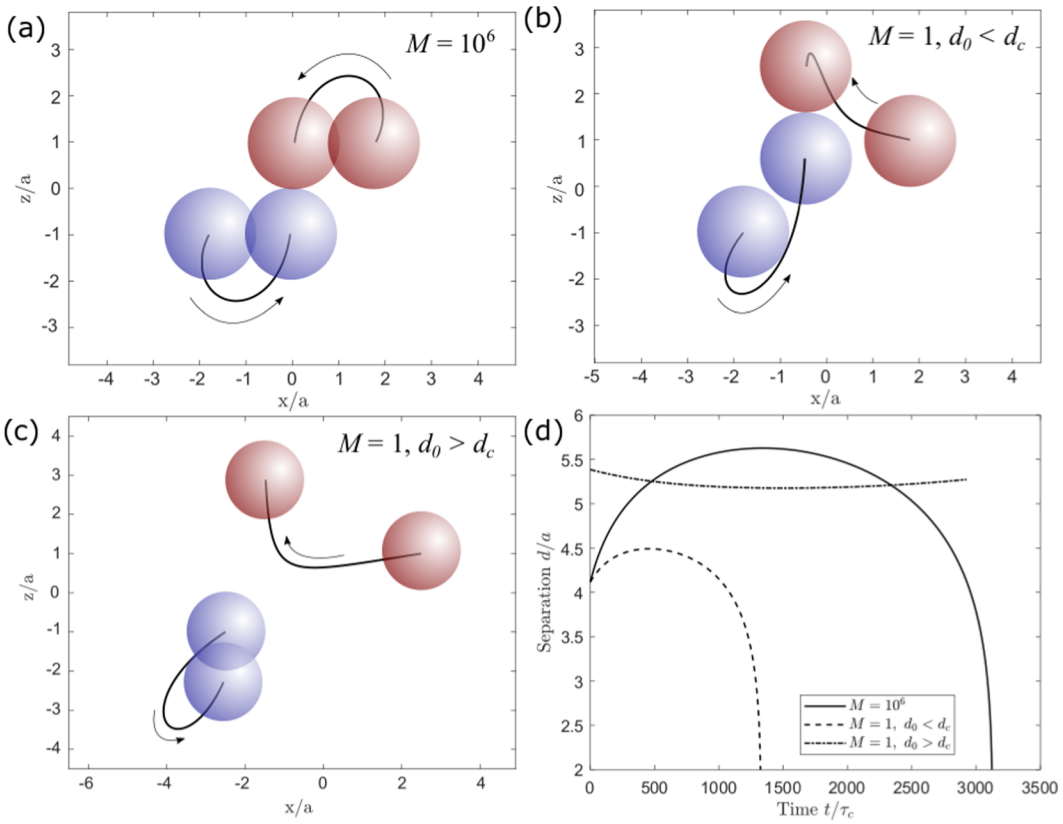

FIG. 10. Trajectories of drops in the plane made by the line connecting the centers of the drops and the field direction. In all cases, $S_{\text{blue}} = S_{\text{red}} = 1$, $R_{\text{blue}} = 10$, $R_{\text{red}} = 0.1$. (a) $M = M_{\text{blue}} = M_{\text{red}} = 10^6$, $d_0/a = 4.1$, $\Theta_0 = 29^\circ$. (b) $M = 1$, $d_0/a = 4.1$, $\Theta_0 = 29^\circ$. (c) $M = 1$, $d_0 = 5.4$, $\Theta_0 = 22^\circ$. (d) Plots of separation distance vs time for the cases (a) (solid line), (b) (dashed line), and (c) (dot-dashed line). For cases (b) and (c), $d_c/a = 5.1$.

the pairwise theory and the three-drop experiment shown in Fig. 11. The success in capturing the separation distances and angles of the vectors $\boldsymbol{d}_{12}$, $\boldsymbol{d}_{23}$, and $\boldsymbol{d}_{13}$ [indicated in Fig. 11(c)] shows that the evolution of the triangle made by the centers of the drops can be predicted up to around 48 s when a doublet between drops 2 and 3 is formed. After formation of the doublet, while still shown for the sake of comparison, the theory is inapplicable, as any lubrication effects that would arise upon near-contact of the drops are ignored, as well as higher-order terms that would increase the accuracy of the model as the drops become close. In any case, the three-body dynamics of this system are successfully captured. To explain this, it is noted that while Eq. (13) is valid for remote separations, higher-order terms for both EHD and DEP come in $O(a/d)^3$ smaller than the terms they are reflected from. Three-body interactions scale similarly, provided the drop sizes are similar, where a third drop of radius a_3 would interact with drop 2 at leading order $O(a_3/d)^2$, which would then reflect to drop 1 at $O(a_3^2 a_2^3/d^5)$ [43]. Thus, by only considering terms up to $O(a/d)^4$, three-body interactions can be ignored, and the pairwise theory of Eq. (17) is accurate to the same order for systems of three drops as it is for a drop pair.

Comparison of the pairwise additive theory to experiments of four drops, as shown in Fig. 12, also shows qualitative agreement. However, while the evolution of the system is captured in this case, considerably faster dynamics are predicted compared to those observed experimentally. For instance, the formation of a drop 2–3 doublet is predicted to occur about twice as fast as seen in the

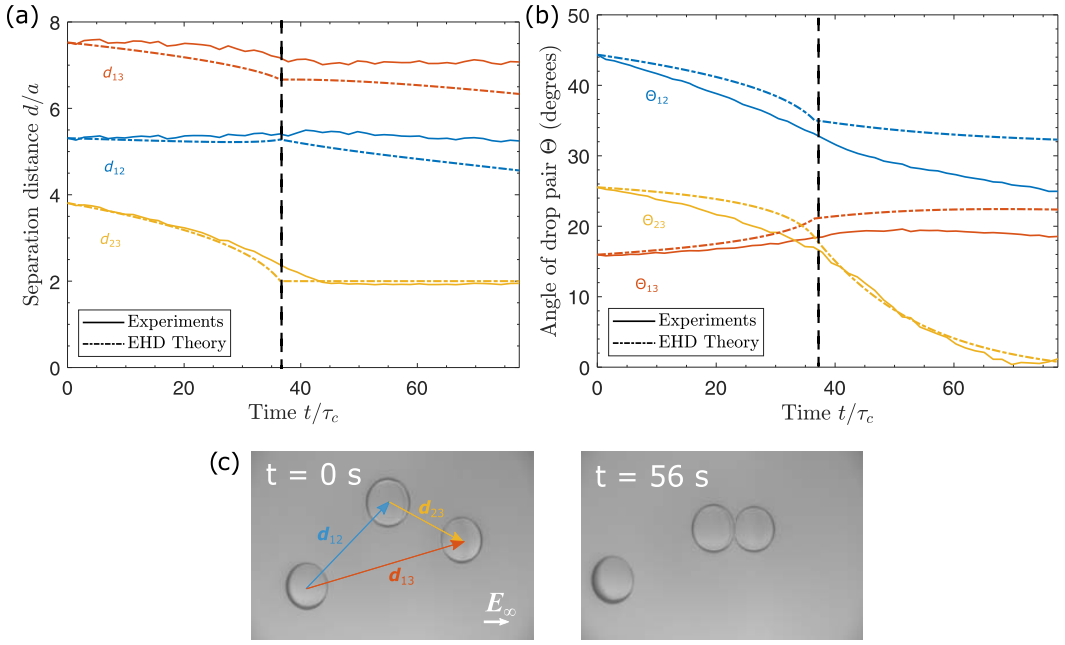

FIG. 11. (a) Separation distance between drop pairs for the three-drop system. (b) Rotational dynamics between drop pairs for the three-drop system. Angles plotted are $|\Theta|$. The vertical dotted line indicates the moment drops 2 and 3 form a doublet, after which the theory is formally inapplicable. The kinks in the theoretical trajectories occur upon predicted formation of the doublet. (c) Photos of the initial and final configuration of drops, with a schematic identifying the vectors plotted in (a) and (b).

experiment, and a similar difference in timescale is observed between the theoretical predictions of the trajectories between the other drops. Considering the quality of agreement in Fig. 11, a likely source of the observed discrepancy in timescale is considered. Based on the observed increase in magnitude of the vector connecting drops 1 and 4, it is possible that the distances from drop 1 to drops 3 and 4, and likewise drop 4 to drops 1 and 2, are large enough such that the interactions along those vectors are small compared to noise from impurities or errant charge in the bulk. Thus, the interactions between drops 1 and 3, drops 1 and 4, and drops 2 and 4 that would in sum be attractive enough to pull drops 1 and 4 together are screened, and the pair of drops 1 and 2 initially repels with minimal interference from the other drops. Combined with the clockwise rotation of the pair of drops 1 and 2 and counterclockwise rotation of the pair of drops 3 and 4, respectively, drops 1 and 4 are driven apart. As a result, as the pair of drops 1 and 2 and the pair of drops 3 and 4 rotate toward parallel, their center-to-center attraction get stronger, slowing the time it would take for drops 2 and 3 to meet. Provided this is the case, the fact that the dynamics of four drops is qualitatively predicted bodes well for prediction of n-body systems of drops, which we plan to address in future work. These results thus show that Eqs. (11), (13), and (17) provide a framework for the approximation of the behavior of large-scale systems of leaky dielectric drops using low-cost simulations compared to more expensive boundary integral codes or multipole expansions incorporating large numbers of terms.

VI. CONCLUSIONS

The three-dimensional interactions of leaky dielectric drops are analyzed using asymptotic analysis and experiments. The theory presented by Sorgentone *et al.* [42] is generalized to consider dissimilar and multiple drops. The interaction parameter Φ is examined, the sign of which is

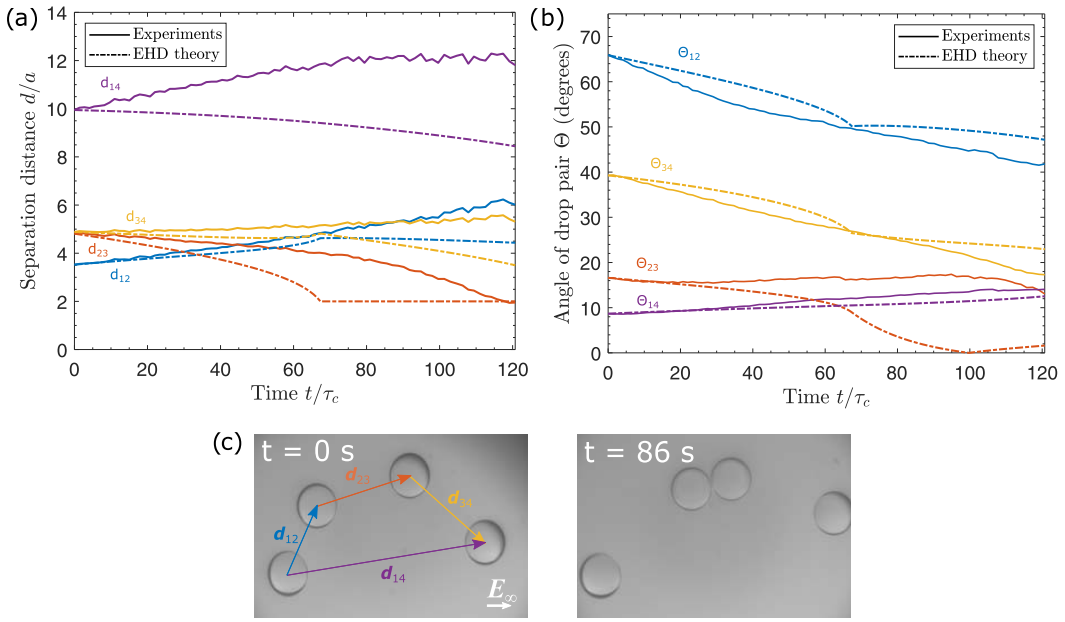

FIG. 12. (a) Separation distance between drop pairs within the four-drop system. (b) Rotational dynamics between drop pairs within the four-drop system. Angles plotted are $|\Theta|$. Here the experiment is stopped upon formation of the doublet between drops 2 and 3, however the theoretical prediction of doublet formation occurs at about 48 s. (c) Photos of the initial and final configuration of drops, with a schematic identifying the vectors plotted in (a) and (b).

predictive of the direction that a drop pair will rotate relative to the field direction. In discussing the possibility of exploring the phase space of Φ in practical systems, it is noted that inherent physical limits on S immediately reduce accessible regions of the Φ phase diagram. Constraints of immiscibility, high surface tension, comparable densities, and similar conductivities in concert make practical realization of predicted yet so far experimentally unobserved drop pair behaviors unlikely in relevant applications.

The theory for identical drops of Sorgentone *et al.* is compared to experiments of silicone oil drops suspended in castor oil, and it is shown that the physics dominant in leaky dielectric drop interactions are captured. The theory is found to accurately predict the trajectories of drop pairs at separation distances as low as 3.5 radii; however, noise in experimental measurements of drop pair interactions may dominate over interaction dynamics at separations larger than 5 radii. Results are shown exemplifying the importance of the angle the drop pair makes with the field direction in determining how quickly drops will attract or repel. Drops are shown to not always interact in a monotonic manner, and the positions of drops at long times are heavily dependent on their initial placement. We find that the theory is successful in qualitatively predicting the dynamics observed in the experiments.

The theory of Sorgentone *et al.* is generalized to consider the asymmetric interactions of widely separated dissimilar drops, and systems of multiple drops through a pairwise additive approximation. Neglecting gravitational effects, it is shown that the theory is capable of predicting the trajectories of drops of different sizes. Simulated trajectories of drops of electrically dissimilar drops are also shown. These nonreciprocal interactions nontrivially impact the predicted trajectories of a drop pair. In cases of three and four drops, a summation of pairwise interactions between drops is shown to qualitatively predict the evolution of the many-body systems. The error in ignoring three-body interactions is of a similar scale to that of the truncation error of $O(a^5/d^5)$ in the pairwise

theory, allowing the use of the pairwise theory to predict the interactions of multiple drops. Although a more rigorous consideration of drop interactions via twin multipole reexpansions or boundary integral computations may provide more accurate resolution of drop interactions at close distances [39,42,52], the simple theory presented here provides a means for qualitatively accurate descriptions of drop interactions at comparatively minuscule computational cost.

While the theory was able to capture the qualitative behavior of drops, our methods can be improved, and a more accurate prediction of drop interactions can be made. Experimentally, we were unable to fully control for migration of the drops or be sure of no errant charges. To mitigate these issues, the needles and oil in the cell were grounded before the experiment and when the drops were inserted and moved, however this was not enough to fully eliminate these effects. It has been suggested that the migration of leaky dielectric drops in a steady field could be electrophoretic in nature [56], and thus could be avoided using an ac field. In terms of the model, we introduce inaccuracy by considering nondeforming drops and ignoring the possibility for charge convection, which we know is relevant at the field strengths used in this study. Additionally, emulsion surfaces are rarely clean, and the presence of surface active species can impact the EHD deformation and interactions of drops [57–59]. Nonetheless, in predicting the interactions of drops in various scenarios using a simple asymptotic theory, a considerable step is taken toward modeling more complex many-body systems. Analogies to our methodology exist in electrocoalescence [36], electrorheology [53], active matter [46,55], and electrokinetics [54], where many-body simulations show a rich depth of behavior not yet quantified for leaky dielectric materials.

ACKNOWLEDGMENTS

We are grateful to C. Sorgentone and P. M. Vlahovska for helpful discussions, and to the anonymous reviewers for their valuable feedback. We thank the National Science Foundation for support through Grant No. CBET-1804548.

[1] J. Melcher and G. Taylor, Electrohydrodynamics: A review of the role of interfacial shear stresses, Annu. Rev. Fluid Mech. **1**, 111 (1969).

[2] D. Saville, Electrohydrodynamics: The Taylor-Melcher leaky dielectric model, Annu. Rev. Fluid Mech. **29**, 27 (1997).

[3] A. M. Ganán-Calvo, J. M. López-Herrera, M. A. Herrada, A. Ramos, and J. M. Montanero, Review on the physics of electrospray: From electrokinetics to the operating conditions of single and coaxial taylor cone-jets, and ac electrospray, J. Aerosol Sci. **125**, 32 (2018).

[4] R. T. Collins, J. J. Jones, M. T. Harris, and O. A. Basaran, Electrohydrodynamic tip streaming and emission of charged drops from liquid cones, Nat. Phys. **4**, 149 (2008).

[5] J. S. Eow and M. Ghadiri, Electrostatic enhancement of coalescence of water droplets in oil: A review of the technology, Chem. Eng. J. **85**, 357 (2002).

[6] K. Aida, Y. H. Na, T. Nagaya, and H. Orihara, Droplet coalescence process under electric fields in an immiscible polymer blend, Phys. Rev. E **82**, 031805 (2010).

[7] J.-W. Ha and S.-M. Yang, Rheological responses of oil-in-oil emulsions in an electric field, J. Rheol. **44**, 235 (2000).

[8] X.-D. Pan and G. H. McKinley, Characteristics of electrorheological responses in an emulsion system, J. Colloid Interface Sci. **195**, 101 (1997).

[9] T. M. Squires and S. R. Quake, Microfluidics: Fluid physics at the nanoliter scale, Rev. Mod. Phys. **77**, 977 (2005).

[10] T. Ward and G. Homsy, Electrohydrodynamically driven chaotic mixing in a translating drop, Phys. Fluids **13**, 3521 (2001).

[11] Z. Rozynek, A. Mikkelsen, P. Dommersnes, and J. O. Fossum, Electroformation of janus and patchy capsules, Nat. Commun. **5**, 3945 (2014).

[12] J.-U. Park, M. Hardy, S. J. Kang, K. Barton, K. Adair, D. K. Mukhopadhyay, C. Y. Lee, M. S. Strano, A. G. Alleyne, J. G. Georgiadis, P. M. Ferreira, and J. A. Rogers, High-resolution electrohydrodynamic jet printing, Nat. Mater. **6**, 782 (2007).
[13] S. N. Jayasinghe, A. N. Qureshi, and P. A. Eagles, Electrohydrodynamic jet processing: an advanced electric-field-driven jetting phenomenon for processing living cells, Small **2**, 216 (2006).
[14] O. A. Basaran, H. Gao, and P. P. Bhat, Nonstandard inkjets, Annu. Rev. Fluid Mech. **45**, 85 (2013).
[15] G. I. Taylor, Studies in electrohydrodynamics. i. the circulation produced in a drop by an electric field, Proc. R. Soc. London A **291**, 159 (1966).
[16] S. Torza, R. Cox, and S. Mason, Electrohydrodynamic deformation and bursts of liquid drops, Philos. Trans. R. Soc. London A **269**, 295 (1971).
[17] J. Sherwood, Breakup of fluid droplets in electric and magnetic fields, J. Fluid Mech. **188**, 133 (1988).
[18] O. A. Basaran, T. W. Patzek, R. E. Benner Jr., and L. Scriven, Nonlinear oscillations and breakup of conducting, inviscid drops in an externally applied electric field, Ind. Eng. Chem. Res. **34**, 3454 (1995).
[19] P. K. Notz and O. A. Basaran, Dynamics of drop formation in an electric field, J. Colloid Interface Sci. **213**, 218 (1999).
[20] E. Lac and G. Homsy, Axisymmetric deformation and stability of a viscous drop in a steady electric field, J. Fluid Mech. **590**, 239 (2007).
[21] A. Esmaeeli and P. Sharifi, Transient electrohydrodynamics of a liquid drop, Phys. Rev. E **84**, 036308 (2011).
[22] P. F. Salipante and P. M. Vlahovska, Electrohydrodynamics of drops in strong uniform dc electric fields, Phys. Fluids **22**, 112110 (2010).
[23] J. A. Lanauze, L. M. Walker, and A. S. Khair, Nonlinear electrohydrodynamics of slightly deformed oblate drops, J. Fluid Mech. **774**, 245 (2015).
[24] R. Sengupta, L. M. Walker, and A. S. Khair, The role of surface charge convection in the electrohydrodynamics and breakup of prolate drops, J. Fluid Mech. **833**, 29 (2017).
[25] D. Das and D. Saintillan, A nonlinear small-deformation theory for transient droplet electrohydrodynamics, J. Fluid Mech. **810**, 225 (2017).
[26] P. M. Vlahovska, Electrohydrodynamics of drops and vesicles, Annu. Rev. Fluid Mech. **51**, 305 (2019).
[27] B. W. Wagoner, P. M. Vlahovska, M. T. Harris, and O. A. Basaran, Electric-field-induced transitions from spherical to discocyte and lens-shaped drops, J. Fluid Mech. **904**, R4 (2020).
[28] A. Marin, The saturnian droplet, J. Fluid Mech. **908**, F1 (2021).
[29] D. Das and D. Saintillan, A three-dimensional small-deformation theory for electrohydrodynamics of dielectric drops, J. Fluid Mech. **914**, A22(2021).
[30] M. Ouriemi and P. M. Vlahovska, Electrohydrodynamic deformation and rotation of a particle-coated drop, Langmuir **31**, 6298 (2015).
[31] H. A. Pohl, Dielectrophoresis, *The Behavior of Neutral Matter in Nonuniform Electric Fields* (Cambridge University Press, New York, 1978).
[32] N. Rivette and J. C. Baygents, A note on the electrostatic force and torque acting on an isolated body in an electric field, Chem. Eng. Sci. **51**, 5205 (1996).
[33] M. Washizu and T. B. Jones, Dielectrophoretic interaction of two spherical particles calculated by equivalent multipole-moment method, IEEE Trans. Ind. Appl. **32**, 233 (1996).
[34] T. B. Jones, *Electromechanics of Particles* (Cambridge University Press, Cambridge, 2005).
[35] P. Atten, Electrocoalescence of water droplets in an insulating liquid, J. Electrost. **30**, 259 (1993).
[36] X. Zhang, O. A. Basaran, and R. M. Wham, Theoretical prediction of electric field-enhanced coalescence of spherical drops, AIChE J. **41**, 1629 (1995).
[37] C. Sozou, Electrohydrodynamics of a pair of liquid drops, J. Fluid Mech. **67**, 339 (1975).
[38] J. C. Baygents, N. Rivette, and H. A. Stone, Electrohydrodynamic deformation and interaction of drop pairs, J. Fluid Mech. **368**, 359 (1998).
[39] M. Zabarankin, Small deformation theory for two leaky dielectric drops in a uniform electric field, Proc. R. Soc. A **476**, 20190517 (2020).
[40] Q. Dong and A. Sau, Electrohydrodynamic interaction, deformation, and coalescence of suspended drop pairs at varied angle of incidence, Phys. Rev. Fluids **3**, 073701 (2018).

[41] S. Mhatre, S. Deshmukh, and R. M. Thaokar, Electrocoalescence of a drop pair, Phys. Fluids **27**, 092106 (2015).
[42] C. Sorgentone, J. I. Kach, A. S. Khair, L. M. Walker, and P. M. Vlahovska, Numerical and asymptotic analysis of the three-dimensional electrohydrodynamic interactions of drop pairs, J. Fluid Mech. **914**, A24 (2021).
[43] S. Kim and S. J. Karrila, *Microhydrodynamics: Principles and Selected Applications* (Courier, Mineola, New York, 2013).
[44] G. Hetsroni and S. Haber, The flow in and around a droplet or bubble submerged in an unbound arbitrary velocity field, Rheol. Acta **9**, 488 (1970).
[45] A. V. Ivlev, J. Bartnick, M. Heinen, C.-R. Du, V. Nosenko, and H. Löwen, Statistical Mechanics Where Newton's Third Law is Broken, Phys. Rev. X **5**, 011035 (2015).
[46] J. Agudo-Canalejo and R. Golestanian, Active Phase Separation in Mixtures of Chemically Interacting Particles, Phys. Rev. Lett. **123**, 018101 (2019).
[47] R. Sengupta, A. S. Khair, and L. M. Walker, Electric fields enable tunable surfactant transport to microscale fluid interfaces, Phys. Rev. E **100**, 023114 (2019).
[48] B. A. Yezer, A. S. Khair, P. J. Sides, and D. C. Prieve, Use of electrochemical impedance spectroscopy to determine double-layer capacitance in doped nonpolar liquids, J. Colloid Interface Sci. **449**, 2 (2015).
[49] J.-W. Ha and S.-M. Yang, Deformation and breakup of newtonian and non-newtonian conducting drops in an electric field, J. Fluid Mech. **405**, 131 (2000).
[50] R. Allan and S. Mason, Particle behaviour in shear and electric fields i. deformation and burst of fluid drops, Proc. R. Soc. London A **267**, 45 (1962).
[51] O. Vizika and D. Saville, The electrohydrodynamic deformation of drops suspended in liquids in steady and oscillatory electric fields, J. Fluid Mech. **239**, 1 (1992).
[52] D. Saintillan, Nonlinear interactions in electrophoresis of ideally polarizable particles, Phys. Fluids **20**, 067104 (2008).
[53] D. Klingenberg, F. Van Swol, and C. Zukoski, Dynamic simulation of electrorheological suspensions, J. Chem. Phys. **91**, 7888 (1989).
[54] J. S. Park and D. Saintillan, Dipolophoresis in large-scale suspensions of ideally polarizable spheres, J. Fluid Mech. **662**, 66 (2010).
[55] C. H. Meredith, P. G. Moerman, J. Groenewold, Y.-J. Chiu, W. K. Kegel, A. van Blaaderen, and L. D. Zarzar, Predator–prey interactions between droplets driven by non-reciprocal oil exchange, Nat. Chem. **12**, 1136 (2020).
[56] O. Schnitzer and E. Yariv, The taylor–melcher leaky dielectric model as a macroscale electrokinetic description, J. Fluid Mech. **773**, 1 (2015).
[57] C. Sorgentone and P. M. Vlahovska, Pairwise interactions of surfactant-covered drops in a uniform electric field, Phys. Rev. Fluids **6**, 053601 (2021).
[58] Y. Han, J. Koplik, and C. Maldarelli, Surfactant and dilatational viscosity effects on the deformation of liquid droplets in an electric field, J. Colloid Interface Sci. **607**, 900 (2022).
[59] J.-W. Ha and S.-M. Yang, Effects of surfactant on the deformation and stability of a drop in a viscous fluid in an electric field, J. Colloid Interface Sci. **175**, 369 (1995).